Influential parameters on submerged discharge capacity of converging ogee spillways based on experimental study and machine learning-based modeling

Kiyoumars Roushangar, Ali Foroudi and Mojtaba Saneie

ABSTRACT

Ogee spillways with converging training walls are applied to lower the hazard of accidental flooding in locations with limited construction operations due to their unique structure. Hence, this type of structure is proposed as an emergency spillway. The present study aimed at experimental and machine learning-based modeling of the submerged discharge capacity of the converging ogee spillway. Two experimental models of Germi-Chay dam spillway were utilized: one model having a curve axis which was made in 1:50 scale and the other with a straight axis in 1:75 scale. Using visual observation, it was found that the total upstream head, the submergence degree, the ogee-crest geometries and the convergence angle of training walls are the crucial factors which alter the submerged discharge capacity of the converging ogee spillway. Furthermore, two machine-learning techniques (e.g. artificial neural networks and gene expression programming) were applied for modeling the submerged discharge capacity applying experimental data. These models were compared with four well-known traditional relationships with respect to their basic theoretical concept. The obtained results indicated that the length ratio ($L2/(L'.Lch)$) had the most effective role in estimating the submerged discharge capacity.

Key words | ANN, artificial neural network, converging ogee spillway, gene expression programing, GEP, submerged discharge capacity

Kiyoumars Roushangar (corresponding author)
Ali Foroudi
Department of Civil Engineering,
University of Tabriz,
Tabriz,
Iran
E-mail: *kroshangar@yahoo.com*

Mojtaba Saneie
Hydraulic Structures, Soil Conservation and Watershed Management Research Institute (SCWMRI),
Agricultural Research Education and Extension Organization (AREEO),
Tehran,
Iran

INTRODUCTION

Accidental flooding of an overflow control structure during large discharge incidents is a common concern. A spillway is a hydraulic structure and a major part of a dam for disposing of flood flows. Dissipation of energy over the spillway usually happens by: (i) a standard stilling basin downstream of the spillway to dissipate energy of flow by forming a hydraulic jump (large amount); (ii) a high velocity water jet taking off from a flip bucket and entering into a downstream plunge pool; and (iii) the construction of steps on the spillway to assist in energy dissipation (Li *et al.* 1989; Roushangar *et al.* 2014).

One of the most common and effective spillways which can pass significant flow with considerably moderate/low construction cost is an ogee spillway. The ogee spillway has a control weir that is ogee shaped ('S' shaped) in profile. The upper curve of the ogee spillway ordinarily conforms closely to the profile of the lower nappe of a ventilated sheet falling from a sharp-crested weir. Flow over the crest adheres to the face of the profile by preventing access of air to the underside of the sheet. For discharges at designed head, the flow glides over the crest with no interference from the boundary surface and attains near maximum

doi: 10.2166/hydro.2019.120

discharge efficiency. The profile below the upper curve of the ogee is a continued tangent along a slope to support the sheet on the face of the overflow (Maynord 1985; EUA-Bureau of Reclamation 1987; USACE 1990; Savage & Johnson 2001; Chatila & Tabbara 2004; Johnson & Savage 2006; Saneie *et al.* 2016). The capacity of the stream of a spillway is determined by the length of the spillway and the shape of the crest. A spillway with an arc in plan has some advantages over straight structures. This kind of spillway increases the length of crest on a given channel width and leads to an increase in flow capacity for a given upstream head. The spillway, therefore, preserves a more constant upstream depth and needs less free board compared with linear weirs (Crookston 2010). To control the upstream water level and increase the flow capacity, the spillway with an arc in plan is often considered to be the desirable option. Due to limits in many geometric design variables, designers may find an optimized design for a particular position challenging, thus physical modeling is used for designing this kind of structure (Johnson & Savage 2006).

So far, some studies have been carried out to investigate the hydraulic properties of ogee spillways and proposed head-discharge relationships, particularly for submerged ogee-crest spillways, e.g. Koloseus (1951), Kline (1953), Collins (1976), Clemmens *et al.* (2001), Kim (2003), Bhajantri *et al.* (2007), Tullis & Neilson (2008), and Mohammadzadeh-Habili *et al.* (2013). In the terms of submerged flow, Ansar & Gonzalez-Castro (2003) investigated submerged weir flow at prototype gated spillways. They developed a submerged weir flow equation based on field measurements collected with an Acoustic Doppler Current Profiler at several prototype gated spillways in southern Florida. Using field flow data at several gated spillways, they have presented the following equation.

$$\frac{y_c}{h} = a\left[\frac{h}{H}\right]^b \tag{1}$$

where h and H are the tailwater and the headwater depth above sill, respectively, a and b are constant, determined from field measurements, as 0.45 and −3.37, respectively and y_c is the critical depth over the sill crest. These measurements showed that the gates had negligible effects on the submerged weir flows when they were not too deep into the water (submergence of the gates less than 20% of the headwater depth). Kabiri-Samani & Javaheri (2012) investigated the effects of the PKW (piano key weir) geometry, including weir length and height, up- and downstream key widths as well as up- and downstream apex overhangs on the weir flow discharge coefficient for both free and submerged flows. On the basis of a comprehensive dataset, they proposed practical discharge coefficient relations associated with the standard weir equation.

However, results of these studies demonstrated that experimental and physical-based equations may lead to incorrect results (Roushangar *et al.* 2014). During recent years, general utilization of machine-learning techniques (e.g. gene expression programming (GEP) and artificial neural networks (ANNs)) in most branches of water engineering (including hydraulics) has become feasible, leading to varied publications in this field (Guven & Gunal 2008; Kisi & Shiri 2011; Karami *et al.* 2012; Shahheydari *et al.* 2015; Nourani *et al.* 2016; Parsaie *et al.* 2016, 2017; Roushangar *et al.* 2018). ANNs have superb performance and have been successfully applied in water resources modeling (Babovic *et al.* 2001). ANNs have also been applied for modeling spillway gates of dams (Bagis & Karaboga 2004), estimating the scour below spillways (Azamathulla *et al.* 2008), determining the flow discharge in straight compound channels (Zahiri & Dehghani 2009), and estimation of scour depth below free over-fall spillways (Samadi *et al.* 2015). In addition, GEP has been applied in modeling wide areas of water engineering systems. For instance, Guven & Azamathulla (2012) employed GEP for predicting scour downstream of a flip-bucket spillway. Moussa (2013) used GEP and ANNs for modeling local scour depth of downstream hydraulic structures in trapezoidal channels. Shiri *et al.* (2013) estimated daily streamflow applying various artificial intelligence techniques and found that GEP performed best. Shiri *et al.* (2014) employed GEP to estimate daily evaporation through spatial and temporal data scanning. Zahiri *et al.* (2014) applied soft computing models to predict local scour depth downstream of bed sills. Bertone *et al.* (2015) applied GEP to model dissolved oxygen (DO) concentration in lakes. Also, Roushangar *et al.* (2016) took advantage of GEP to estimate scour depth downstream of grade-control structures. Baxgatur &

Onen (2016) employed GEP to develop predictive models for flood routing. Roushangar *et al.* (2014) applied GEP and ANN approaches for modeling energy dissipation over stepped spillways and the results demonstrated that the application of GEP and ANN in these cases are very favorable and encouraging.

To the authors' knowledge, there is a deficiency in evaluation of submerged discharge of converging ogee spillways based on machine-learning techniques, since this type of spillway has unique design and construction properties, especially for cases with limited construction operations, where selected spillway width cannot be the same size in up and downstream (e.g. smaller width of crest on the downstream is necessary). Therefore, in this research, the discharge of the converging ogee spillway under submerged flow conditions is assessed experimentally and the effects of various variables on Q_s (submerged flow capacity) are studied. On the other hand, this study aimed to assess the capability of GEP and ANN approaches for modeling the discharge of the converging ogee spillway under submerged flow conditions (Q_s). The models were prepared under various input combinations (based on the hydraulic characteristics and geometry of the spillway) in order to find the most appropriate input combination for modeling. Furthermore, GEP-based practical formulas of Q_s were proposed and these models were compared with ANN-based and experimental models for submerged discharge relationships of the ogee spillway. For this end, the methods presented by Skogerboe *et al.* (1967), Varshney & Mohanty (1973), Cox (1928) and EUA-Bureau of Reclamation (1987) were applied to estimate the *Qs*.

MATERIAL AND METHODS

Experimental details

In this study, two experimental models of Germi-Chay Mianeh dam spillway were utilized, one model having a curve axis that was made in 1:50 scale and the other with a straight axis fabricated in 1:75 scale. The Soil Conservation and Watershed Management Research Institute (SCWMRI) in Tehran, Iran performed the research effort on converging ogee spillways of the dam. Table 1 summarizes the design parameters for the models of converging ogee spillway design in 3D scale as well as prototype design parameters for these structures. The curve axis model was tested with both symmetrical and asymmetrical convergence of training walls, where the model with a straight axis was only investigated using symmetrical conditions. The range of convergence angle (θ) for both models was limited to $0 < \theta < 120°$. Figures 1 and 2 illustrate a schematic of the two models and four samples of the converging ogee spillway, respectively.

In the physical model with a straight axis at 1:75 scale, a reservoir of length 4 m, width 0.7 m and depth 0.5 m was used. The other physical model with a curve axis at 1:50 scale was located at the outlet of a rectangular flume 3.00 m long, 0.8 m wide, 0.4 m high. Before the test area,

Table 1 | Models and prototype design parameters and dimensions

Design elements	Prototype dimensions	Model dimensions Curve axis model Scale 1:50					Straight axis model Scale 1:75		
Convergence angles (°)	120 sym	120 sym	90 sym	90 asym	60 sym	60 asym	120 sym	90 sym	60 sym
($L2/(L'.Lch)$)	5.56	5.565	4.467	3.836	3.469	2.999	4.667	3.946	3.211
Crest length, L (m)	42	0.837	0.712	0.628	0.578	0.51	0.56	0.4735	0.3853
Design discharge ($m^3 s^{-1}$)	398	0.0225	0.0182	0.0183	0.0158	0.01404	0.0059	0.0054	0.0048
Maximum discharge ($m^3 s^{-1}$)	717	0.0405	0.0344	0.0304	0.028	0.0247	0.0146	0.01245	0.01005
Maximum head (m)	5	0.1					0.0667		
Spillway height (m)	7.8	0.156					0.104		
Design head (m)	3	0.06					0.04		
Downstream channel width (m)	9	0.18					0.12		

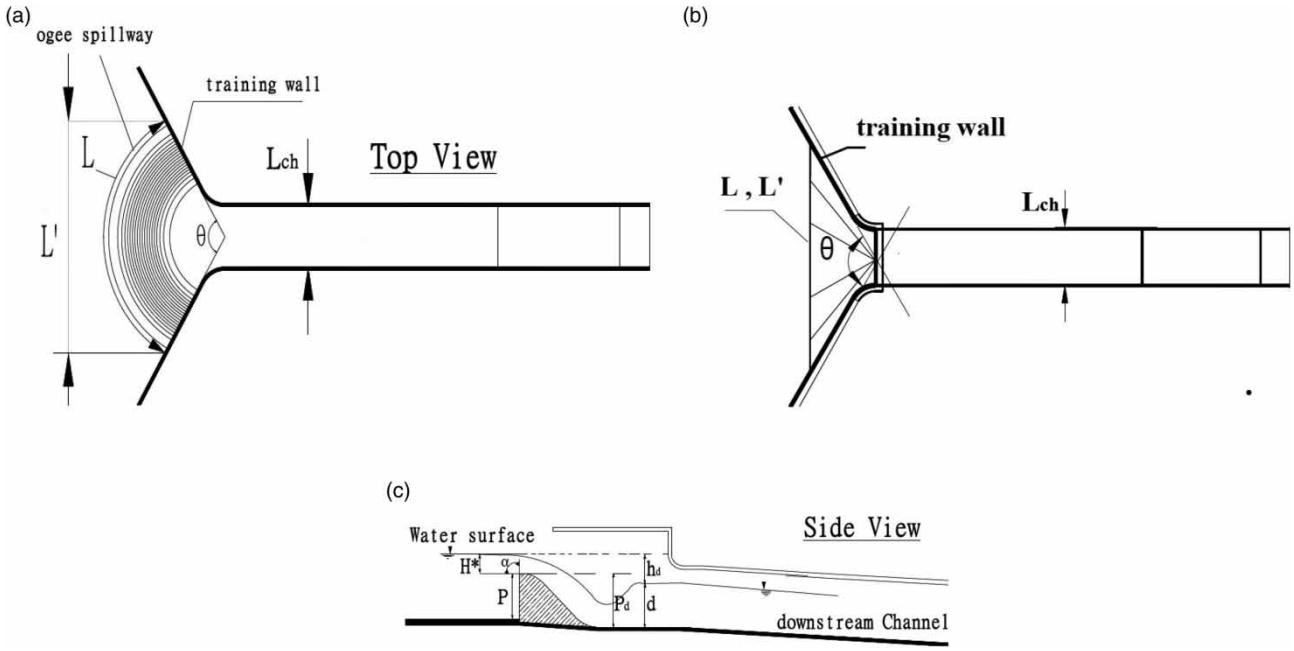

Figure 1 | Schematic of typical converging ogee spillways with (a) curve axis, (b) straight axis, and (c) side view of spillways.

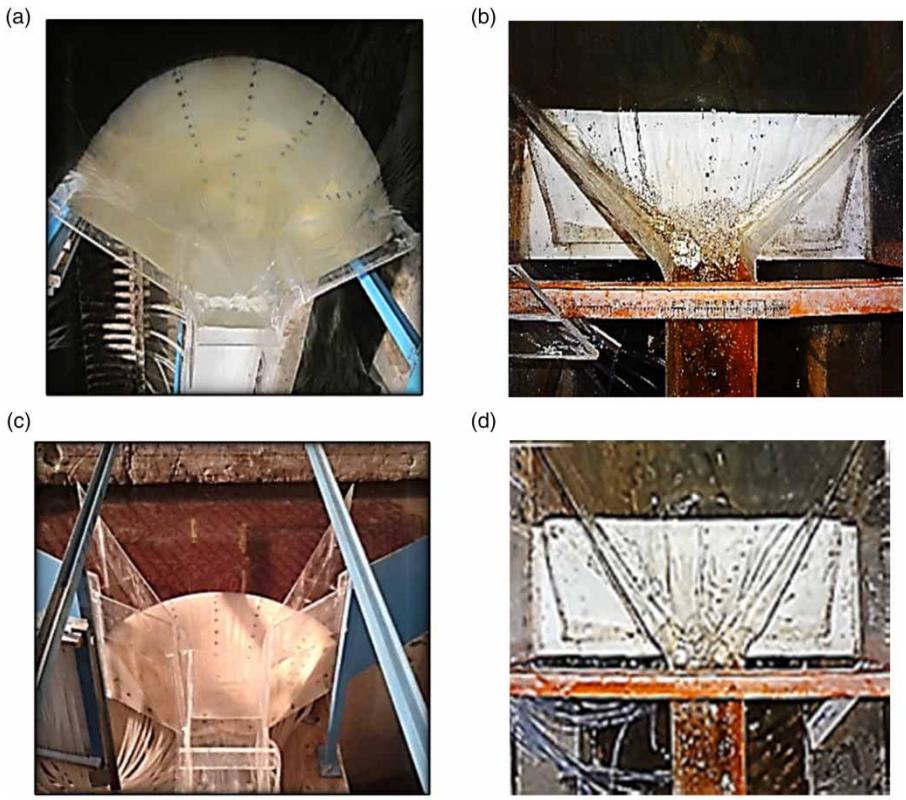

Figure 2 | Photographs of the spillways with convergence angles of (a) 120° symmetric (curve axis), (b) 120° symmetric (straight axis), (c) 60° symmetric (curve axis), and (d) 60° asymmetric (straight axis).

the flume was equipped with an adequate stilling structure to reach the steady approach flow. Discharge was measured utilizing a sharp triangular weir with an apex angle of 90° in the output channel throughout the experiment. The measurements of flow depth were obtained using a point gauge with ±1.0 mm reading accuracy. As a result of water surface fluctuation, average values of free surface elevations were collected based on many measurements. Froude Number similarity is generally applied for scale relationships between the model and prototype, since the impact of gravity is typically more important compared with the impact of viscosity and surface tension for these types of models (EUA-Bureau of Reclamation 1980). Therefore, Froude similarity was employed in the present study.

Dimensional analysis for submerged discharge capacity (Q_s)

Discharge capacity of an ogee-crested spillway for free flow conditions can be expressed as (EUA-Bureau of Reclamation 1987):

$$Q_f = \frac{2}{3} C_d \sqrt{2g} L H^{3/2} \tag{2}$$

where C_d = free flow discharge coefficient, g = the gravitational acceleration, L = crest length, and H = discharge head on the spillway. When tailwater exceeds a certain level above the spillway crest elevation, spillway submergence occurs. The discharge capacity over an ogee spillway under submerged flow conditions might be considered as a function of the geometric parameters and flow characteristic. A functional relationship linking the main parameters of flow over the converging ogee spillway can be expressed as

$$f_1(Q_s, H^*, L, P, P_d, H_d, g, \rho, \mu, \sigma, h_d, \alpha, \theta) = 0 \tag{3}$$

where f_1 is a functional symbol; H^* and H_d are the total submerge-flow upstream head and the design head, respectively; P and P_d, are the ogee crest upstream and downstream spillway heights, respectively; μ and ρ are dynamic viscosity and density, respectively; h_d is the height difference between the height of ogee spillway crest and flow depth on downstream; α is the slope of the upstream face of spillway; σ is the surface tension and θ is the convergence angle of training walls. Equation (3) represents a physical phenomenon. Centered on the Buckingham Π theorem, this equation may be expressed in a dimensionless form as

$$\Pi_1 = f_2(\Pi_2, \Pi_3, \Pi_4, \Pi_5, \Pi_6, \Pi_7, \Pi_8, \Pi_9, \Pi_{10}) \tag{4}$$

in which Π_1, Π_2, Π_3, Π_4, Π_5, Π_6, Π_7, Π_8, Π_9 and Π_{10} are the dimensionless groups and f_2 is a functional symbol. Considering Q, H^* and ρ as dimensional independent parameters as well as mentioned parameters suggested by Featherstone & Nalluri (1982), the non-dimensional groups were computed as

$$\Pi_1 = \frac{Q_s}{g^{0.5} H^{*1.5}},\ \Pi_2 = \frac{H^*}{p},\ \Pi_3 = \frac{H^*}{H_d},\ \Pi_4 = \frac{h_d}{H^*},$$
$$\Pi_5 = \frac{P_d + h_d}{H^*}, \Pi_6 = \frac{L}{H^*}, \Pi_7 = \frac{\mu}{\rho g^{0.5} H^{*1.5}},\ \Pi_8 = \frac{\sigma}{\rho g H^{*2}},$$
$$\Pi_9 = \theta, \Pi_{10} = \alpha \tag{5}$$

Considering that some groups must be combined to deduce the dimensionless parameters commonly applied in hydraulics, Equation (4) is expressed in the form

$$\Pi_1 = f_3\left(\Pi_2, \Pi_3, \Pi_4, \Pi_5, \Pi_6, \frac{1}{\Pi_7}, \Pi_8, \Pi_9, \Pi_{10}\right) \tag{6}$$

Substituting Π_1, Π_2, Π_3, Π_4, Π_5, Π_6, Π_7, Π_8 and Π_9 from Equation (5) into Equation (6) brings

$$\frac{Q_s}{g^{0.5} H^{*1.5}} = f_3\left(\frac{H^*}{p}, \frac{H^*}{H_d}, \frac{h_d}{H^*}, \frac{P_d + h_d}{H^*}, \frac{L}{H^*}, \frac{\rho g^{0.5} H^{*1.5}}{\mu}, \frac{\sigma}{\rho g H^{*2}}, \theta, \alpha\right) \tag{7}$$

where f_3 is a functional symbol. The seventh and the eighth terms on the right-hand side shows the Reynolds number R and the Weber number W, respectively. For the all performed experiments that $H > 30$ mm, the possible effects of surface tension on discharge are small and hence analysis of Weber number was removed from analysis (Novak & Cabelka 1981). Moreover, since the flow is in turbulent condition, the viscosity effect is small compared with gravity. Based on this description, the effect of the Reynolds number was also omitted from the further analysis (Henderson 1966). Furthermore, the ogee-shaped crest has a vertical upstream slope, so it has no significant effect on

the discharge coefficient. The submergence degree (S) is introduced as the level difference between reservoir and tailwater to the total upstream head on the spillway (hd/H); thus, hd/H was substituted with S. In the present study, two experimental models were used: one model having a curved axis which was tested in both symmetrical and asymmetrical converging training walls (θ's), and the other with a straight axis which was only investigated with symmetrical converging training walls. Thus, the dimensionless parameter $\frac{L^2}{L'.L_{ch}}$ was used by considering both of the impact of curved or straight crest axis and symmetric or asymmetric situations for each of the tested θ's, where L' (m) and L_{ch} (m) are the length of straight line between the two ends of the crest curve and the downstream channel width, respectively (both in meter). Consequently, Equation (7) may be expressed as

$$Q_s = g^{0.5} H^{*1.5} f\left(\frac{H^*}{H_d}, \frac{H^*}{p}, S, \frac{P_d + H^*}{H^*}, \frac{L}{H^*}, \frac{L^2}{L'.L_{ch}}\right) \quad (8)$$

Finally, Equation (8) is expressed in the next form

$$Q_s = \Phi\left(\frac{H^*}{H_d}, \frac{H^*}{p}, S, \frac{P_d + H^*}{H^*}, \frac{L}{H^*}, \frac{L^2}{L'.L_{ch}}\right) \quad (9)$$

where Φ is another functional symbol.

Machine learning-based modeling

Gene expression programming

GEP technique applied in the current study is a developed version of genetic algorithm (GA) and genetic programming (GP) (Holland 1975) and is an approach used for learning the best 'fit' programs via artificial evolution (Johari *et al.* 2006). The GEP method advanced by Ferreira (2001) is an extension of genetic algorithms (GAs) (Goldberg 1989). In the process of modeling discharge capacity via GEP, optimum parameters were selected and applied several times to find the best outcome. It should be remarked that the present procedure is based on the investigations through using the complete dataset to select the appropriate operators per run. Consequently, all selected input variables were introduced as input space of the GEP and the effect of various GEP operators on results were analyzed through the statistical indexes introduced. The first step with investigations on GEP operators is the selection of the appropriate fitness function. So, the default basic function set of *GeneXpro* program (i.e., +, −, ×, /, $\sqrt{}$, $\sqrt[3]{}$, ln, e^x, x^2, x^3, sin x, cos x, *Arctgx*) was used with the complete dataset (as input variables) for the selecting fitness function. The chronological set of experimental data was then divided into two separate groups randomly (approximately 75% vs. 25%; which is usual in literature for ordinary cross-validation) to evaluate the developed GEP models with independent vectors.

In GEP, a mathematical function is described as a chromosome with multiple genes, and developed using the data presented to it. The procedure for predicting submerged discharge capacity of converging ogee spillway is as follows. There are five crucial stages in the application of GEP. The first stage is the fitness function (Ferreira 2006). In order to select suitable fitness function, a trial-and-error procedure was applied. Based on the results, the Root Mean Square Error (RMSE) fitness function was chosen (not presented here). The second stage includes choosing the set of terminals, T, and the operation function set, F, to generate the chromosomes. In the present study, the terminal set includes $\frac{H^*}{H_d}$, $\frac{H^*}{p}$, S, $\frac{P_d + H^*}{H^*}$, $\frac{L}{H^*}$ and $\frac{L^2}{L'.L_{ch}}$. The choice of the appropriate function depends on the specific problem studied. In this study, a range of basic functions were investigated but those investigated systematically are given below:

$$F1 = \{+, -, \times, \div\}$$

$$F2 = \{+, -, \times, \div, \sqrt{}, X^2\}$$

$$F3 = \{+, -, \times, \div, \sqrt{}, Power, Lnx, Logx, e^x, 10^x\}$$

$$F4 = \{+, -, \times, \div, \sqrt{}, Power, Lnx, Logx, e^x, \sin x, \cos x, Arctg\, x\}$$

$$F5 = \{+, -, \times, \div, \sqrt[3]{}, \sqrt{}, Lnx, e^x, X^2, X^3, \sin x, \cos x, Arctg\, x\}$$

According to the outcome of present study and approved by the results reported by various researchers (Kisi & Shiri 2011; Roushangar *et al.* 2014, 2016), it is deduced

that the first function set (F1) has demonstrated superiority to the other applied function sets; thus, the F1 set will be employed in the above-mentioned stages.

The third stage is to select the chromosomal architecture. The architecture of the chromosomes including number of chromosomes (25–30–35), head size (7–8) and number of genes (3–4), were selected and different combinations of the mentioned parameters were tested. The model was run for a number of generations and was stopped when there was no significant change in the fitness function value and coefficient of correlation. It is observed that the model with 30 chromosomes, head size 8, and 3 genes yielded better results.

The fourth important stage is selecting the linking function. Based on the results of works in related field and results of modeling of real-valued GEP in the present study (trial-and-error process for different structures), it was observed that addition-linking function demonstrated superiority to the other linking functions and hence was selected as optimum linking function in the present study (e.g. Ferreira 2001, 2002; Kisi & Shiri 2011).

The fifth and final stage is to select the set of genetic operators. In the present study a combination of all genetic operators (recombination, mutation, transposition, and crossover) was employed towards this aim. The rates of genetic operators which determine a certain probability of a chromosome were determined using a trial-and-error process. Each GEP model was evolved (trained model) until there was no significant change in the fitness function value, then the program was stopped (fixed model). Therefore, the GEP model optimized parameters were determined. The related parameters applied per run are summarized in Table 2.

Table 2 | Parameters of the GEP model applied in present study

Parameters	Definition	Setting of parameter
P1	Function set	$+, -, *, /, \sqrt{}, x^2$
P2	Chromosomes	30
P3	Head size	8
P4	Number of genes	3
P5	Linking function	Addition
P6	Fitness function	Root mean square error (RMSE)
P7	Mutation rate	0.044
P8	Inversion rate	0.1
P9	One-point recombination rate	0.3
P10	Two-point recombination rate	0.3
P11	Gene recombination rate	0.1
P12	Gene transposition rate	0.1

Artificial neural network

ANN is a computing framework that is able to simulate a large amount of complex nonlinear processes (Haykin & Cybenko 1999), which relate the inputs and outputs of any system. The parameters to be detected by training are the weight vectors, which connect to the different nodes of the input, hidden, and output layers of the network by the commonly named error-back-propagation approach (Haykin & Cybenko 1999). During training, the values of the weights parameter are altered; thus, the ANN output becomes similar to the measured output on an identified dataset. Theoretical works have affirmed that one hidden layer is adequate for ANNs to predict any complex nonlinear mathematical function (Haykin & Cybenko 1999). So, in this study, one hidden layer was applied to build the ANN organization (Rumelhart *et al.* 1986; Roushangar *et al.* 2018). Here, the hidden layer node numbers of each model are determined after trying various network structures since there is no theory yet to tell how many hidden units are needed to approximate any given function (trial-and-error process led to better results without facing an over-fitting situation). To determine the optimal network, many designs were tried whereby the hidden layer neuron numbers varied from 1 to 9 (1, 2, 3 … 9). For the hidden and output node activation functions, the tangent sigmoid function and pure linear transfer functions are found suitable, respectively. Feed-Forward-Back Propagation, Levenberg–Marquardt algorithm (LMA) and gradient descent momentum were employed for neural network type, training function and adoption learning function, respectively. The training of the ANN technique was stopped when the error of the calibration stage started to increase. All the model construction processes was performed by applying MATLAB software.

Classical submerged discharge capacity methods

Four methods were found in the literature for predicting head-discharge relationships for submerged ogee-crest weir. There are different concepts and approaches that are used in the derivation and extraction processes of these formulas. The utilized experimental formulas in this study are as follows.

Formula of Cox

Cox (1928) performed experimental submergence tests with various ogee-crest geometries and proposed a relationships for submerged flow conditions as:

$$Q_s = \frac{2}{3} C_s \sqrt{2g} L H^n \tag{10}$$

The independent parameters in Cox's formula would be the weir height (P), measured in meters, and submergence degree (S). Cox demonstrated that the following relationships are only usable in the validity range of submergence degree (S) from 0.6 to 0.9,

$$C_s = 3.895 + 0.3490814P - \frac{(1.52 - 0.1886\sqrt{0.3048P})S^2}{1.433 - 0.004123944P - S} \tag{11}$$

$$n = 1.625 + \frac{0.036}{\sqrt{0.3048P}} - \frac{\left(\frac{0.428}{0.3048P - 0.169} - 0.0129\right)S^2}{0.886 + \frac{4.2979}{P} - S} \tag{12}$$

Formula of Skogerboe *et al.*

Skogerboe *et al.* (1967) modified a submerged head-discharge relationship extended for Parshall and cut-throat flumes to submerged ogee-crest weirs applying the Koloseus (1951) dataset.

$$Q_s = \frac{1.048512\, L(0.3048h^* - 0.3048h_d)^{1.69}}{\left\{-\left[log_{10}\left(\frac{h_d}{h^*}\right) + 0.0025\right]\right\}^{1.20}} \tag{13}$$

where Q_s is measured in cubic meter per second ($m^3\,s^{-1}$) and L, h^*, and h_d in feet. The submergence degree (S) used ranged from 0.5 to 0.95.

Formula of Varshney and Mohanty

Varshney & Mohanty (1973) developed an experimental formula for describing submerged head-discharge relationships to a wide variety of broad crested weirs, comprising ogee-crests. The application of Equation (14) was limited to $0.65 < S < 1.0$.

$$\frac{Q_s}{Q_f} = \sqrt{-7.75s^2 + 9.81s - 2.26} \tag{14}$$

Formula of EUA-Bureau of Reclamation (Bradley 1945)

Bradley (1945) discovered that Q_s was a function of S, P, and the height of downstream weir (P_d). Bradley developed graphical relationships, demonstrating the reduction in the C_s, relative to C_f at a common upstream head, is caused by variations in H_d, P, and P_d. Bradley's relationships were located into the ogee-crest weir design technique published in the *Design of Small Dams* (EUA-Bureau of Reclamation 1987). To the best of the authors' knowledge, none of the research reviewed presented statements considering the predictive ability of the individual method (i.e., the ability of the predictive relationship to match experimentally determined Q_s values).

Performance criteria

In this study, the performance of models is evaluated in terms of three statistical parameters, i.e. R (Pearson's correlation coefficient), Coefficient of Determination (COD), and the RMSE:

$$\mathrm{R} = \frac{\sum_{i=1}^{N}(o_i - \overline{o_i}) \times (t_i - \overline{t_i})}{\sqrt{\sum_{i=1}^{N}(o_i - \overline{o_i})^2 \sum_{i=1}^{N}(t_i - \overline{t_i})^2}} \tag{15}$$

$$COD = 1 - \frac{\sum_{i=1}^{N}(O_i - t_i)^2}{\sum_{i=1}^{N}(O_i - \overline{O_i})^2} \tag{16}$$

$$RMSE = \sqrt{\frac{\sum_{i=1}^{N}(O_i - t_i)^2}{N}} \tag{17}$$

where O_i and t_i represent the measured and estimated submerged discharge capacity values, respectively, while $\overline{Oi}$ and $\overline{ti}$ denote the mean of the measured and predicted values, respectively, N represents the number of data samples, R provides information for linear dependence between observations and corresponding simulated values and should not be employed alone as a performance criterion (Roushangar *et al.* 2017; Farajzadeh & Alizadeh 2018). *RMSE* describes the average magnitude of the errors by attributing more weight to large errors. *COD* is applied to show the relative assessment of the model performance in dimensionless measures (Nourani *et al.* 2016). Higher values of R and *COD* and lower values of *RMSE* means are intended to determine the best model.

RESULTS AND DISCUSSION

In this study, two experimental models of Germi-Chay Mianeh dam spillway were used; one model with a curved axis was made in 1:50 scale and the other with a straight axis was made in 1:75 scale. It seems that differences between these two experimental models from a physical scale point of view, leads to the difference between the measured data and the prototype. Nonetheless, Saneie *et al.* (2016) demonstrated that for submergence conditions having the minimum Reynolds and Weber numbers which are 3.1×10^4 and 270, respectively, and $We^{0.6}Re^{0.2} > 300$, it is possible to neglect the effect of viscosity and surface tension in a converging ogee spillway (Saneie *et al.* 2016). As an example, Table 3 shows a sample angle (120°) in 1:50 and 1:75 scales in which the conditions required by Saneie *et al.* (2016) to omit the scale effect were satisfied. Also, according to Equations (18) and (19) which were proposed by Saneie *et al.* (2016) for the discharge coefficient in converging ogee spillways, K' is a parameter to amend the scale effect. According to Figure 3, K' is equal to 1 and thereby, simply the scale effect can be omitted from upcoming analysis. Equations (18) and (19) are as follows:

$$C_d = (0.611 + 0.075H/W)K' \tag{18}$$

$$K' = 0.94 + \frac{33.02}{Re^{0.2}We^{0.6}} \tag{19}$$

Table 3 | Conditions required by Saneie *et al.* (2016) to omit the scale effect

θ	H/W	Re	We	$Re^{0.2}$ $We^{0.6}$
120, scale 1:50	0.473	5.83×10^4	636.0	431.7764
	0.488	6.10×10^4	675.5	451.7538
	0.503	6.39×10^4	718.2	473.0031
	0.531	6.94×10^4	801.2	513.4626
	0.568	7.67×10^4	915.3	567.3779
	0.598	8.29×10^4	1,015.8	613.4813
	0.637	9.11×10^4	1,151.3	673.8686
	0.668	9.78×10^4	1,266.3	723.7452
	0.705	1.06×10^5	1,411.5	785.1435
	0.745	1.15×10^5	1,576.3	852.92
	0.772	1.22×10^5	1,695.2	900.7406
120, scale 1:75	0.558	4.09×10^4	396.2	302.7682
	0.610	4.67×10^4	472.8	345.7043
	0.666	5.33×10^4	564.1	394.6593
	0.704	5.79×10^4	629.5	428.4762
	0.731	6.13×10^4	678.5	453.287
	0.802	7.05×10^4	817.9	521.4441
	0.847	7.65×10^4	913.1	566.3567
	0.894	8.29×10^4	1,015.8	613.484
	0.947	9.04×10^4	1,140.2	669.0056

where K' is a function of Reynolds number and Weber number, H is head over the spillway crest and W is spillway elevation (m).

Figures 4 and 5 show Reynolds (*Re*) and Weber (*We*) numbers, respectively, to water elevation on spillway crest divided by spillway elevation (H/W). It can be seen from these figures that the minimum Reynolds and Weber numbers are higher than 3.1×10^4 and 270, respectively, and thus, in this research the effect of viscosity and surface tension in physical models were neglected. According to this

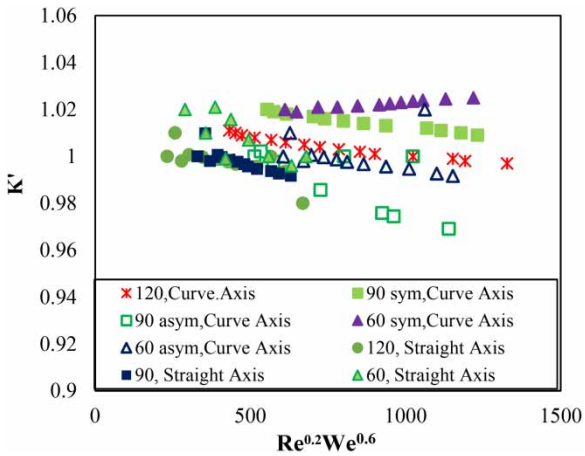

Figure 3 | Conditions required by the study of Saneie *et al.* (2016) to omit the scale effect.

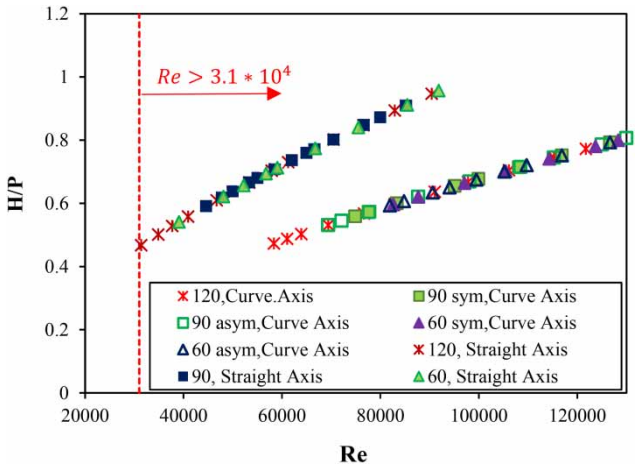

Figure 4 | Reynolds number diagram to water elevation on the spillway crest.

fact, obtained results from the physical models which have been simulated applying Froude simulation can be extrapolated to the prototype.

As the tailwater exceeds the crest elevation, the converging spillway becomes less efficient due, in part, to the local submergence downstream. In this situation, a minimum S level is required before conditions at the critical section are influenced and the free-flow head-discharge relationship no longer applies. Using the test data, various rating curves were generated for Q_s. Note that all relationships for Q_s are almost nonlinear. Figures 6 and 7 show the variations of Q_s in relation to various dimensionless parameters of Equation (9). Changes in Q_s for varying θ's are presented against H^*/P in Figure 6(a). The vertical aspect ratio H^*/P has two expressible effects: (1) it reflects the effect of the approach flow head for a fixed height of spillway; and (2) it shows the

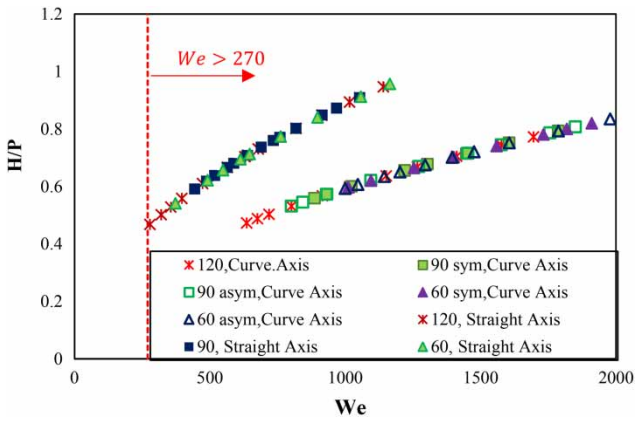

Figure 5 | Weber number diagram to water elevation on the spillway crest.

effect of the spillways with different heights for a constant approaching discharge head. In this research, the results obtaining for two models from constant P, but different H^* indicate that Q_s increases with increasing approaching flow head. However, it seems that increase in the slope for Q_s vs. H^*/P of spillway with a straight axis has been consistently higher than the spillway with a curved axis. This could be caused by almost all of the upstream flow lines in the curved axis model having been trained perpendicular to the crest axis by training walls, while in the straight axis model a portion of upstream flow lines near the training walls have deviations from the hypothetical perpendicular line to the crest axis and causes it explicitly to pass flows.

The variation of Q_s for varying θ's are demonstrated versus (H^*/H_d) in Figure 6(b) indicating that a decrease in θ, or in other words the decrease in the ratio $\frac{L2}{L'.Lch}$, leads to a noticeable increase in Q_s. For the straight axis model, the submerged discharge starts at 389 $cm^3\ s^{-1}$ with $H^*/H_d = 1.24$ and with $H^*/H_d = 2.52$, increases to 920 $cm^3\ s^{-1}$, while for the curved axis model discharge starts at 476 $cm^3\ s^{-1}$ with $H^*/H_d = 1.14$ and with $H^*/H_d = 2.41$ rises to 948 $cm^3\ s^{-1}$. It seems that for the straight axis model the increase in discharge slope was higher than that in the curved axis model and demonstrates better hydraulic performance of this model due to the higher flow passing over the spillway in the certain upstream head compared with the curved axis model.

Figure 6(c) shows the discharge coefficient variation affected by tailwater conditions (C_s) for various values of Q_s for both models indicating that increasing Q_s decrease C_s. Note that in the straight axis model, the convergence angle of 60° with $\frac{L2}{L'.Lch} = 3.21$ is the optimal value in terms of C_s because of the significant effect of L against L_{ch}, whereby C_s increases if the downstream channel width is increased. For the curve axis model, the convergence angle variation $\left(\frac{L2}{L'.Lch}\right)$ has a marginal effect on the discharge coefficient. However, $\frac{L2}{L'.Lch} = 5.56$ has the least effect from this point of view.

Figure 7(a) is a plot of downstream apron conditions $(P_d + H^*)/H^*$ on the discharge capacity. The results indicate that

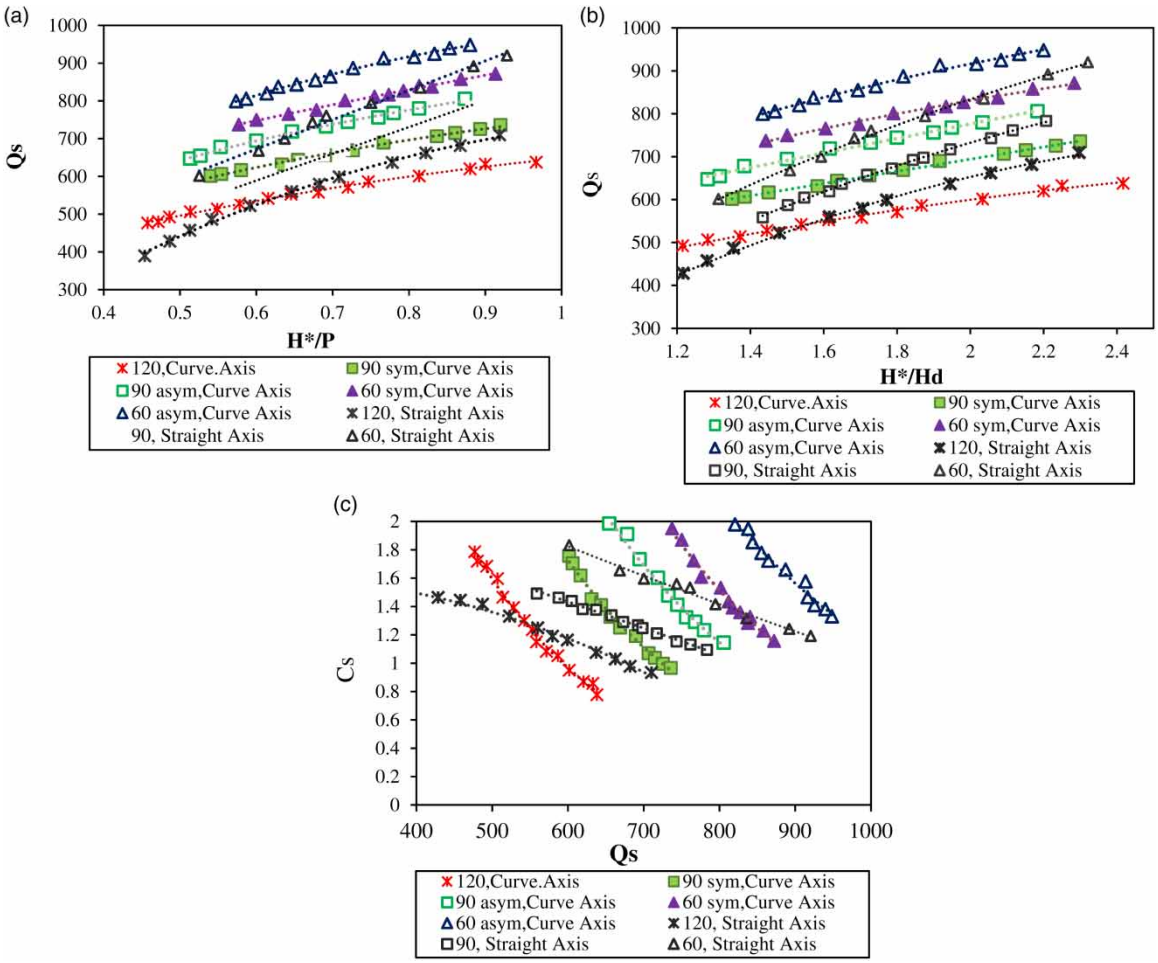

Figure 6 | Comparison of submerged discharge capacity of two physical models for varying θ against (a) H^*/P, (b) H^*/H_d, and (c) C_s.

decreasing $(P_d + H^*)/H^*$ produces a higher Q_s for two models. The effects of the tailwater submergence on Q_s were investigated by comparing Q_s versus S for different values of θ (Figure 7(b)), indicating that increasing S produces a higher Q_s for each of the two models. Nonetheless, it can be concluded from Figure 7(a) and 7(b) that discharge capacity changes versus S and $(P_d + H^*)/H^*$ are inversely related; in other words for both models, increasing Q_s tends to increase S and decrease $(P_d + H^*)/H^*$, respectively. Moreover, as the downstream channel width (L_{ch}) increases, the overall effect of the submergence degree (S) associated with the downstream apron values $(P_d + H^*)/H^*$ decreases and the flow passing over the spillway increases. Accordingly, a converging spillway with a smaller $\frac{L2}{L'.Lch}$ ratio performs better.

Machine learning-based modeling

In the current study, GEP- and ANN-based models were developed for predicting the submerged discharge of a converging ogee spillway. Eighteen models with different input combinations were employed using the dimensionless parameters mentioned in Equation (9) (see Table 4). A trial-and-error procedure was employed to obtain the best separation of dataset for training and testing stages. This procedure is done to determine the best performance criteria, so four partitioning modes were considered that include 65–35 (i.e. 65% of data for training and 35% of them for testing dataset), 70–30, 75–25, and 80–20 modes. Among the partitioning modes, separating datasets approximately 75–25 showed the best result. So, in both machine learning-based models, approximately 75% of observed experimental

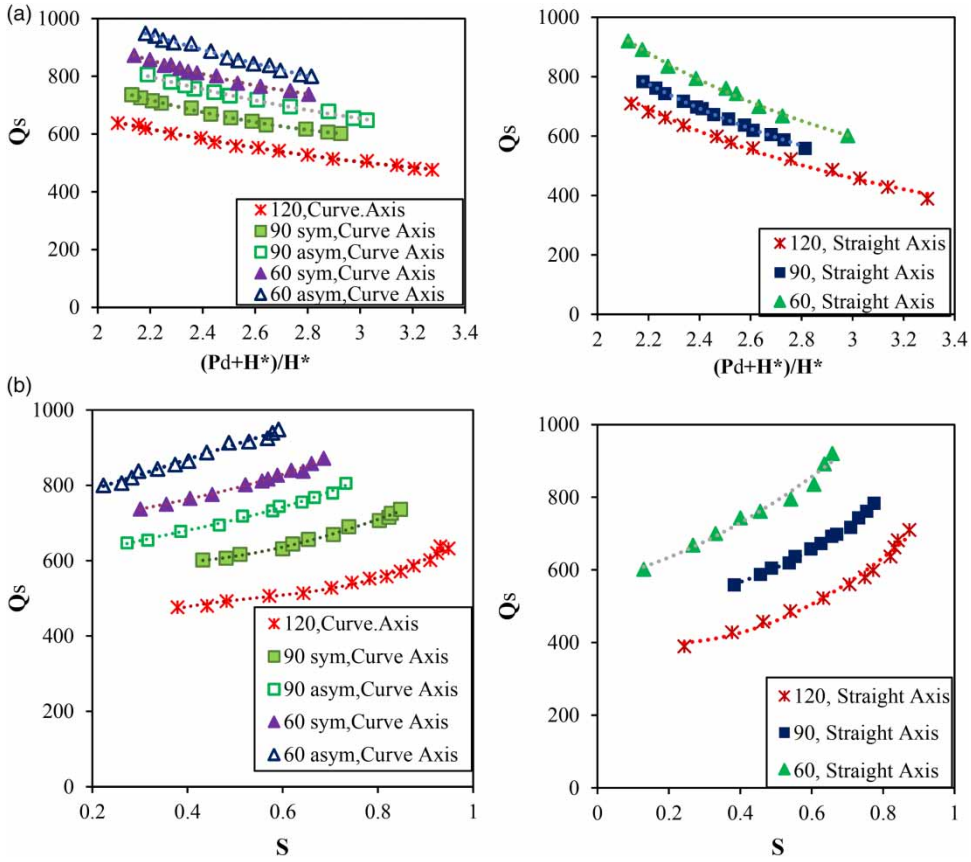

Figure 7 | Ratio of submerged discharge capacity caused by (a) position of downstream apron effects and (b) tailwater effects.

data were employed for training and the remaining 25% selected for testing. Accordingly, 72 datasets (75% of data) were selected for training and 25 datasets (25% of remained data) for simulation were selected for both GEP and ANN models randomly. As demonstrated in Table 4, M1 to M18 input datasets were fed into GEP and ANN models to predict the variable of interest.

Table 5 shows the results of statistical parameters of the first- and second-best models for both training and testing phases per model (GEP and ANN).

Table 4 | Developed input dataset configurations

Model	Input variables	Model	Input variables	Model	Input variables
M1	$\left(S, \frac{H^*}{H_d}, \frac{H^*}{p}, \frac{L}{H^*}, \frac{P_d+H^*}{H^*}, \frac{L^2}{L'.L_{ch}}\right)$	M7	$\left(\frac{H^*}{H_d}, \frac{H^*}{p}, \frac{P_d+H^*}{H^*}, \frac{L^2}{L'.L_{ch}}\right)$	M13	$\left(\frac{H^*}{H_d}, \frac{H^*}{p}, \frac{P_d+H^*}{H^*}\right)$
M2	$\left(S, \frac{H^*}{H_d}, \frac{L}{H^*}, \frac{P_d+H^*}{H^*}, \frac{L^2}{L'.L_{ch}}\right)$	M8	$\left(\frac{H^*}{H_d}, \frac{H^*}{p}, \frac{P_d+H^*}{H^*}, \frac{L^2}{L'.L_{ch}}\right)$	M14	$\left(\frac{H^*}{p}, \frac{P_d+H^*}{H^*}, \frac{L^2}{L'.L_{ch}}\right)$
M3	$\left(S, \frac{H^*}{H_d}, \frac{H^*}{p}, \frac{L}{H^*}, \frac{L^2}{L'.L_{ch}}\right)$	M9	$\left(S, \frac{H^*}{H_d}, \frac{P_d+H^*}{H^*}\right)$	M15	$\left(S, \frac{H^*}{p}, \frac{L^2}{L'.L_{ch}}\right)$
M4	$\left(S, \frac{H^*}{H_d}, \frac{H^*}{p}, \frac{P_d+H^*}{H^*}, \frac{L^2}{L'.L_{ch}}\right)$	M10	$\left(S, \frac{H^*}{H_d}, \frac{L^2}{L'.L_{ch}}\right)$	M16	$\left(S, \frac{P_d+H^*}{H^*}, \frac{L^2}{L'.L_{ch}}\right)$
M5	$\left(S, \frac{H^*}{H_d}, \frac{P_d+H^*}{H^*}, \frac{L^2}{L'.L_{ch}}\right)$	M11	$\left(S, \frac{P_d+H^*}{H^*}, \frac{L^2}{L'.L_{ch}}\right)$	M17	$\left(S, \frac{L^2}{L'.L_{ch}}\right)$
M6	$\left(S, \frac{H^*}{H_d}, \frac{H^*}{p}, \frac{L^2}{L'.L_{ch}}\right)$	M12	$\left(\frac{H^*}{H_d}, \frac{H^*}{p}, \frac{L^2}{L'.L_{ch}}\right)$	M18	(S)

Table 5 | Statistics of the two best models

		Training			Testing			
Applied model	**Model**	***R***	***COD***	***RMSE***	***R***	***COD***	***RMSE***	**ANN configns**
ANN	M16	0.997	0.994	9.63	0.998	0.976	36.58	3-7-1
	M5	0.981	0.963	23.59	0.979	0.946	31.11	4-6-1
GEP	M5	0.967	0.936	31.32	0.965	0.926	36.58	–
	M17	0.973	0.948	28.09	0.966	0.924	36.99	–

It can be clearly seen from Table 5 that ANN-based M16 model with 3-7-1 configurations (i.e. 3, 7 and 1 identified input pattern data, neuron in hidden layer and output pattern data, respectively) offer the most accurate performance to estimate submerged discharge capacity (Q_s). On the other hand, GEP-based M5 model provides the second best model with relatively low error and high correlation values among all GEP-based models. It should be noted that one of the key superiorities of the GEP approach over the other machine learning models (e.g., ANN) is providing developed mathematical expressions for the investigated phenomenon which describes the relationship between input and output variables. Mathematical expressions of the M5 and M17 models areas follows.

M5 model:

$$Q_s = \frac{85.963809\frac{P_d+H^*}{P}\left(14.371245+\frac{L^2}{L'.L_{ch}}\right)}{\frac{L^2}{L'.L_{ch}}} + \frac{\frac{L^2}{L'.L_{ch}}\left(2.477936-2\frac{L^2}{L'.L_{ch}}\right)}{3.098144S^2} + \frac{-11.421427*\frac{P_d+H^*}{H^*}\left(2S+\frac{P_d+H^*}{H^*}-\frac{L^2}{L'.L_{ch}}\right)}{\frac{P_d+H^*}{H^*}-\frac{H^*}{p}} + \frac{L^2}{L'.L_{ch}} - 3.098144 \quad (20)$$

M17 model:

$$Q_s = \frac{S^2+0.232941S-44.39758974736}{0.02174997} + \frac{3051.641891}{\frac{L^2}{L'.L_{ch}}} + \frac{\left(\frac{L^2}{L'.L_{ch}}\right)^3}{4.325439} + \frac{S-4.586212}{\frac{L^2}{L'.L_{ch}}-4.586212} \quad (21)$$

The question that then poses itself is that of the meaning or 'semantic content' of these expressions. By answering this question, researchers will be able to interpret and obtain additional insight on influential parameters of the above-mentioned term (Q_s). Equations (20) and (21) outperform the human-generated formulation, and are at the same time rich in meaning. For example, the dimensionless term S is effectively a ratio of flow characteristics and geometric parameters. The geometric parameters are represented by h_d responsible for downstream apron conditions, while the total upstream head H^* is 'responsible' for total energy of flow discharge. Moreover, the non-dimensional parameters of ratios $\frac{H^*}{p}$ and $\frac{P_d+H^*}{H^*}$ are responsible for total energy of flow discharge and downstream floor position, respectively. Also, the remaining group $\frac{L^2}{L'.L_{ch}}$ is a length ratio which responds to represent the impact of geometric parameters of spillway and connected downstream channel as an effective term for expressing the submerged discharge formula. Furthermore, the above-mentioned formulae are dimensionless and they use the most relevant physical properties in the relevant context. By utilizing dimensionless values, problems related to units of measurement, which is a strong reason for the transformation, were avoided. Many researches in the field of hydraulic science reveal that scientists indeed follow this approach, which is part of standard scientific practice (Babovic & Keijzer 2000; Babovic 2009). Figure 8 illustrates the observed versus corresponding simulated values of the submerged discharge using the best GEP and ANN models. In current research, test plots show that desired performance is provided with GEP and ANN, where ANN performed better than GEP.

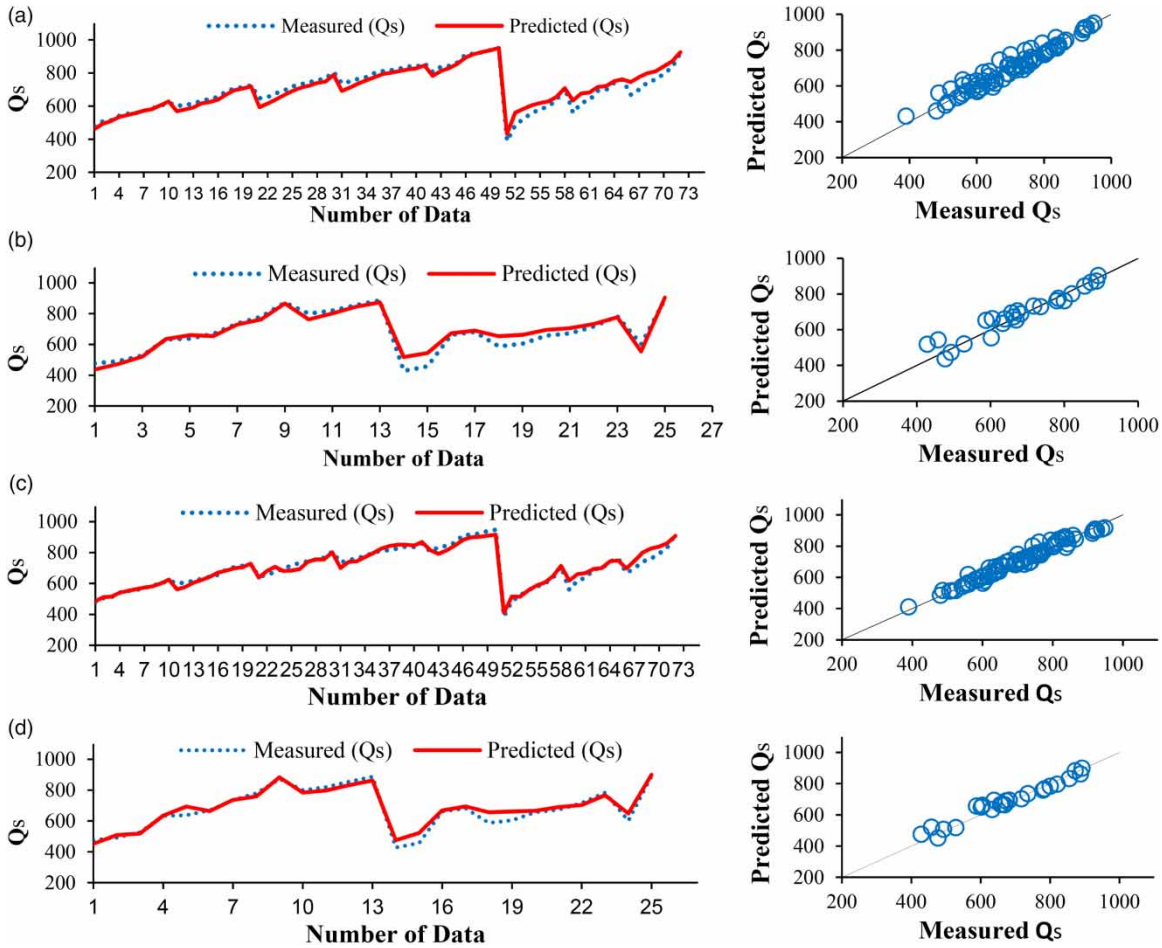

Figure 8 | Measured and predicted Q_s using the best model (M5): (a) GEP training set; (b) GEP testing set; (c) ANN training set; and (d) ANN testing set.

Sensitivity analysis

To derive the most effective parameters on submerged discharge prediction, a sensitivity analysis was performed on both machine-learning models (ANN and GEP). To perform sensitivity analysis, the model M16 was considered. Following this, the significance of each applicable variable was assessed by eliminating them individually. Clearly, deleting each parameter causes an influence in the performance of machine-learning models. The results of sensitivity analysis of both models are presented in Table 6. Reviewing Table 6 shows that elimination of the length ratio $\left(\frac{L2}{L'.Lch}\right)$ causes a considerable decrease in the accuracy of model. Hence, it was concluded that this parameter has the most significant effect on predicting the submerged discharge of a converging ogee spillway in M16 model. On the other hand, elimination of the downstream apron conditions $(P_d + H^*)/H^*$ causes a minimal reduction in the accuracy of model. Thus, it was found that this parameter has a minor effect on submerged discharge capacity in the best model (M13).

Comparison of ANN, GEP and submerged ogee spillway discharge methods

The present study took advantage of both experimental and theoretical-based results in order to select dominant parameters affecting submerged discharge capacity of converging ogee spillways (dimensional and dimensionless). Some other studies have also approved the methods applied

Table 6 | Result of sensitivity analysis for M16 model

			ANN			GEP		
Absent	**Inputs**	**Output**	***R***	***COD***	***RMSE***	***R***	***COD***	***RMSE***
—	$\left(S, \frac{P_d+H^*}{H^*}, \frac{L^2}{L'.L_{ch}}\right)$	Q_s	0.988	0.976	20.838	0.962	0.921	36.72
S	$\left(\frac{P_d+H^*}{H^*}, \frac{L^2}{L'.L_{ch}}\right)$		0.969	0.935	34.217	0.947	0.892	44.274
$\frac{P_d+H^*}{H^*}$	$\left(S, \frac{L^2}{L'.L_{ch}}\right)$		0.98	0.951	29.836	0.966	0.924	36.994
$\frac{L^2}{L'.L_{ch}}$	$\left(S, \frac{P_d+H^*}{H^*}\right)$		0.948	0.887	45.246	0.93	0.862	49.973

here (Tullis 2010; Keijzer & Babovic 2002; Meshgi *et al.* 2005; Tullis & Nilson 2008; Kabiri-Samani & Javaheri 2012; Mohammadzadeh-Habili *et al.* 2013). Support vector machine (SVM)-based models performed relatively weakly for dimensional models. Therefore, an attempt was made to use dimensionless variables to amend the performance of models.

Dimensional analysis is a well-established modeling technique which employs domain knowledge in form of the physical dimensions of the model parameters. The physical dimension information about the model parameters is used to reduce the combinatorial complexity in the search for the correct model. The transfer of similarity methods from engineering to artificial intelligence-based models is possible because both domains share common objects, such as real-world data. The use of group transforms, as formally guaranteed by the Buckingham π Theorem, is therefore straightforward in the modeling of many real-valued artificial intelligence techniques. The results provide some insight into the modeling power of dimensional analysis in an SVM model. The use of group transforms as formally guaranteed by the Buckingham π Theorem is therefore straightforward in the modeling of real-valued artificial intelligence techniques (Rudolph 1997; Najafzadeh *et al.* 2014).

Accuracy of the best proposed models developed in this study, and some head-discharge relationships for submerged ogee-crest weir available in literature were compared to evaluate the performance of the applied approach. The results of comparison for any dataset and overall procedure for two physical models are represented in Figure 9. According to three statistical evaluation criteria (*R*, *COD* and *RMSE*) depicted in Figure 9, it can be shown that the predicted values via ANN and GEP models led to more accurate results than other applied methods. It should be noted that existing equations are developed based on a special validity range of submergence degree (*S*), therefore, the number of datasets in each method is not the same. The mentioned issue can be seen in Figure 9, which depicts that the range of obtained results from equations differ from each other and from the proposed model in this research. In the current study, the method presented by Skogerboe *et al.* (1967) and Varshney & Mohanty (1973) underestimated *Qs*, whereas the methods presented by Cox (1928) and EUA-Bureau of Reclamation (1987) overestimated the *Qs*. Moreover, the method proposed by Skogerboe *et al.* (1967) showed slightly better results than other proposed relationships for submerged discharge capacity and thus, the Skogerboe *et al.* (1967) formula had a more accurate outcome. It should be noted that the current research supplements traditional methods by using proposed formulae for submerged discharge capacity of ogee spillways especially for ogee spillways with special geometry conditions (converging training walls). The obtained results confirmed the capability of GEP and ANN as machine-learning models in the estimation of discharge capacity of a converging ogee spillway.

CONCLUSIONS

Converging ogee spillway is an important hydraulic structure and can be built as an emergency spillway on a

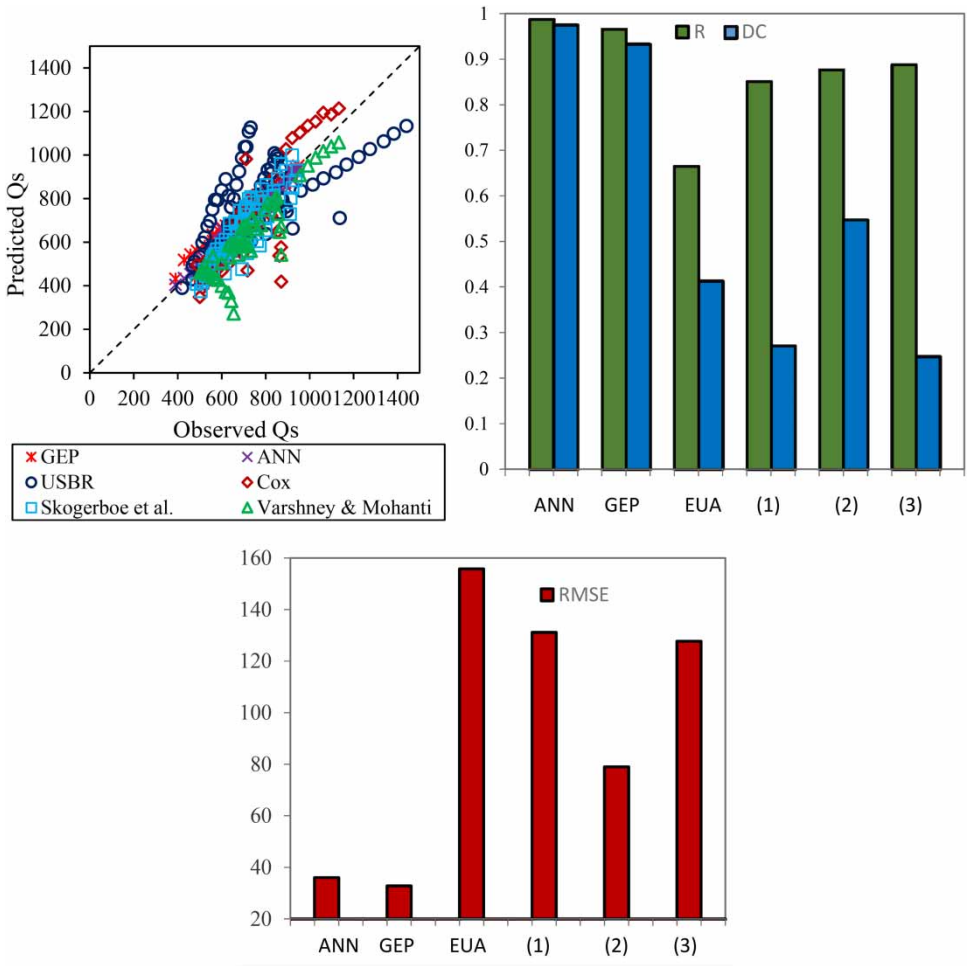

Figure 9 | Comparison of experimental equations and machine-learning models for predicting submerged discharge capacity ((1) Cox (1928); (2) Skogerboe *et al.* (1967); (3) Varshney & Mohanty (1973)).

variety of sites which have potential for coincidental flooding. In this study, the impact of the variation of each of its flow characteristics and spillway geometries on the submerged discharge capacity were assessed. Results demonstrated that an increase in discharge (submerged condition) led to a lower discharge coefficient. This condition could be due to occurrence of tailwater submergence in higher submergence degrees. Moreover, it can be concluded from the results of this study that discharge capacity changes versus S and $(P_d + H^*)/H^*$ which are inversely related; in other words for both models an increase in Q_s tends to increase S and decrease $(P_d + H^*)/H^*$. Furthermore, experiments indicated that as θ or $\frac{L2}{L'.Lch}$ decreases, the overall effect of the submergence degree (S) loss associated with the downstream apron values $(P_d + H^*)/H^*$ decreases and the discharge passing over the spillway increases. In other words, C_s increases if the downstream channel width is increased. By using results of the experimental study, two different machine learning-based approaches are utilized to predict the discharge capacity of the converging ogee spillway for submerged flow conditions. The above-mentioned dataset was the basis of modeling via artificial neural networks (ANNs) and gene expression programming (GEP) techniques. Moreover, the efficiencies of four submerged discharge relationships for ogee-crest in estimating discharge values (Q_s) were assessed. Comparison of the achieved results by two machine learning-based models affirm their capability and competency as efficient techniques in predicting the submerged discharge capacity of the converging ogee spillway and results showed that

ANN and GEP led to more accurate outcomes than other conventional methods. The developed GEP equations provide a simple and practical way for submerged discharge capacity prediction and supplement traditional methods particularly for ogee spillways with special geometric properties. Based on the obtained results from sensitivity analysis, $\frac{L2}{L'.Lch}$ was shown to have the most effective role in predicting the submerged discharge capacity of the converging ogee spillway.

REFERENCES

Ansar, M. & Gonzalez-Castro, J. A. 2003 Submerged weir flow at prototype gated spillways. In: *World Water & Environmental Resources Congress*, 23–26 June, Philadelphia, Pennsylvania, USA, pp. 1–6.

Azamathulla, H. M., Deo, M. & Deolalikar, P. 2008 Alternative neural networks to estimate the scour below spillways. *Advances in Engineering Software* **39**, 689–698.

Babovic, V. 2009 Introducing knowledge into learning based on genetic programming. *Journal of Hydroinformatics* **11**, 181–193.

Babovic, V. & Keijzer, M. 2000 Genetic programming as a model induction engine. *Journal of Hydroinformatics* **2** (1), 35–60.

Babovic, V., Caňizares, R., Jensen, H. R. & Klinting, A. 2001 Neural networks as routine for error updating of numerical models. *Journal of Hydraulic Engineering* **127**, 181–193.

Bagis, A. & Karaboga, D. 2004 Artificial neural networks and fuzzy logic based control of spillway gates of dams. *Hydrological Processes* **18**, 2485–2501.

Baxgatur, T. & Onen, F. 2016 Computation of design coefficients in ogee-crested spillway structure using GEP and regression models. *KSCE Journal of Civil Engineering* **20**, 951–959.

Bertone, E., Stewart, R. A., Zhang, H. & Veal, C. 2015 Data-driven recursive input–output multivariate statistical forecasting model: case of DO concentration prediction in Advancetown Lake, Australia. *Journal of Hydroinformatics* **17**, 817–833.

Bhajantri, M., Eldho, T. & Deolalikar, P. 2007 Modeling hydrodynamic flow over spillway using weakly compressible flow equations. *Journal of Hydraulic Research* **45**, 844–852.

Bradley, J. N. 1945 *Studies of Flow Characteristics, Discharge and Pressures Relative to Submerged Dams*. US Department of the Interior, Bureau of Reclamation, Washington, DC, USA.

Chatila, J. & Tabbara, M. 2004 Computational modeling of flow over an ogee spillway. *Computers and Structures* **82**, 1805–1812.

Clemmens, A. J., Wahl, T. L., Bos, M. G. & Replogle, J. A. 2001 *Water Measurement with Flumes and Weirs*. International Institute for Land Reclamation and Improvement, ILRI, Wageningen, The Netherlands.

Collins, D. L. 1976 Discharge computations at river control structures. *Journal of the Hydraulics Division* **102**, 845–863.

Cox, G. N. 1928 The submerged weir as a measuring device. *Bulletin of the University of Wisconsin*, Engineering Experiment Station Series No. 67, University of Wisconsin, Madison, WI, pp. 1–153.

Crookston, B. M. 2010 *Labyrinth Weirs*. Paper 802. Graduate Theses and Dissertations, Utah State University, Utah, USA.

EUA-Bureau of Reclamation 1980 *Hydraulic Laboratory Techniques*, 2nd edn. Government Printing Office, Denver, CO, USA.

EUA-Bureau of Reclamation 1987 *Design of Small Dams*, 3rd edn. Government Printing Office, Denver, CO, USA.

Farajzadeh, J. & Alizadeh, F. 2018 A hybrid linear–nonlinear approach to predict the monthly rainfall over the Urmia Lake watershed using wavelet-SARIMAX-LSSVM conjugated model. *Journal of Hydroinformatics* **20**, 246–262.

Featherstone, R. E. & Nalluri, C. 1982 *Civil Engineering Hydraulics: Essential Theory with Worked Examples*. Granada Publishing, Spain.

Ferreira, C. 2001 Algorithm for solving gene expression programming: a new adaptive problems. *Complex Systems* **13**, 87–129.

Ferreira, C. 2002 Gene expression programming in problem solving. In: *Soft Computing and Industry*. Springer, Berlin, pp. 635–653.

Ferreira, C. 2006 *Gene Expression Programming: Mathematical Modeling by an Artificial Intelligence*. Springer, Berlin.

Goldberg, D. E. 1989 *Genetic Algorithm in Search, Optimization and Machine Learning*. Addison-Wesley Longman, Boston, MA, USA.

Guven, A. & Azamathulla, H. M. 2012 Gene-expression programming for flip-bucket spillway scour. *Water Science and Technology* **65** (11), 1982–1987.

Guven, A. & Gunal, M. 2008 Genetic programming approach for prediction of local scour downstream of hydraulic structures. *Journal of Irrigation and Drainage Engineering* **134**, 241–249.

Haykin, S. & Cybenko, G. 1999 Approximation by superposition of a sigmoidal function neural networks. *Math. Control Signals Syst.* **2**, 303–314.

Henderson, F. M. 1966 *Open Channel Flow*. Prentice-Hall, Englewood Cliffs, NJ, USA.

Holland, J. H. 1975 *Adaptation in Natural and Artificial Systems. An Introductory Analysis with Application to Biology, Control, and Artificial Intelligence*. University of Michigan Press, Ann Arbor, MI.

Johari, A., Habibagahi, G. & Ghahramani, A. 2006 Prediction of soil–water characteristic curve using genetic programming. *Journal of Geotechnical and Geoenvironmental Engineering* **132**, 661–665.

Johnson, M. C. & Savage, B. M. 2006 Physical and numerical comparison of flow over ogee spillway in the presence of tail water. *Journal of Hydraulic Engineering ASCE* **132**, 1353–1357.

Kabiri-Samani, A. & Javaheri, A. 2012 Discharge coefficients for free and submerged flow over Piano Key weirs. *Journal of Hydraulic Research* **50**, 114–120.

Karami, H., Ardeshir, A., Saneie, M. & Salamatian, S. A. 2012 Prediction of time variation of scour depth around spur dikes using neural networks. *Journal of Hydroinformatics* **14**, 180–191.

Keijzer, M. & Babovic, V. 2002 Declarative and preferential bias in GP-based scientific discovery. *Genetic Programming and Evolvable Machines* **3**, 41–79.

Kim, N. 2003 *Investigation of Scale Effects of Hydraulic Model for dam Spillway Using 3-D CFD Model*. Dissertation. Dept. of Civil Engineering, Seoul National University, Seoul, Korea.

Kisi, O. & Shiri, J. 2011 Precipitation forecasting using wavelet-genetic programming and wavelet-neuro-fuzzy conjunction models. *Water Resources Management* **25**, 3135–3152.

Kline, S. J. 1953 The description of uncertainties in single sample experiments. *Mech. Eng.* **75**, 3–9.

Koloseus, H. J. 1951 *Discharge Characteristics of Submerged Spillways*. PhD thesis, Colorado Agricultural and Mechanical College, CO, USA.

Li, W., Xie, Q. & Chen, C. J. 1989 Finite analytic solution of flow over spillways. *Journal of the Engineering Mechanics Division ASCE* **115**, 2635–2648.

Maynord, S. T. 1985 *General Spillway Investigation*. Technical Report No. HL-85-1. Dept. of the Army, Waterways Experiment Station, Corps of Engineers, Vicksburg, Miss.

Meshgi, A., Schmitter, P., Chui, T. F. M. & Babovic, V. 2005 Development of a modular streamflow model to quantify runoff contributions from different land uses in tropical urban environments using genetic programming. *Journal of Hydrology* **525**, 711–723.

Mohammadzadeh-Habili, J., Heidarpour, M. & Afzalimehr, H. 2013 Hydraulic characteristics of a new weir entitled of quarter-circular crested weir. *Flow Measurement and Instrumentation* **33**, 168–178.

Moussa, Y. A. M. 2013 Modeling of local scour depth downstream hydraulic structures in trapezoidal channel using GEP and ANNs. *Ain Shams Engineering Journal* **4**, 717–722.

Najafzadeh, M., Barani, G. A. & Hessami Kermani, M. R. 2014 Estimation of pipeline scour due to waves by GMDH. *Journal of Pipeline Systems Engineering and Practice* **5**, 06014002.

Nourani, V., Alizadeh, F. & Roushangar, K. 2016 Evaluation of a two-stage SVM and spatial statistics methods for modeling monthly river suspended sediment load. *Water Resources Management* **30**, 393–407.

Novak, P. & Cabelka, J. 1981 *Models in Hydraulic Engineering*. Pitman, London, UK.

Parsaie, A., Haghiabi, A. H., Saneie, M. & Torabi, H. 2016 Prediction of energy dissipation on the stepped spillway using the multivariate adaptive regression splines. *ISH Journal of Hydraulic Engineering* **22**, 281–292.

Parsaie, A., Azamathulla, H. M. & Haghiabi, A. H. 2017 Prediction of discharge coefficient of cylindrical weir-gate using GMDH-PSO. *Journal of Hydraulic Engineering* **24**, 116–123.

Roushangar, K., Akhgar, S., Salmasi, F. & Shiri, J. 2014 Modeling energy dissipation over stepped spillways using machine learning approaches. *Journal of Hydrology* **508**, 254–265.

Roushangar, K., Akhgar, S., Erfan, A. & Shiri, J. 2016 Modeling scour depth downstream of grade-control structures using data driven and empirical approaches. *Journal of Hydroinformatics* **18**, 946–960.

Roushangar, K., Garekhani, S. & Alizadeh, F. 2017 Forecasting daily seepage discharge of an earth dam using wavelet–mutual information–gaussian process regression approaches. *Geotechnical and Geological Engineering* **34**, 1313–1326.

Roushangar, K., Alizadeh, F. & Nourani, V. 2018 Improving capability of conceptual modeling of watershed rainfall–runoff using hybrid wavelet-extreme learning machine approach. *Journal of Hydroinformatics* **20**, 69–87.

Rudolph, S. 1997 On topology, size and generalization of non-linear feed-forward neural networks. *Neurocomputing* **16**, 1–22.

Rumelhart, D. E., Hinton, G. E. & McClelland, J. L. 1986 A general framework for parallel distributed processing. *Parallel Distributed Processing: Explorations in the Microstructure of Cognition* **1**, 45–76.

Samadi, M., Jabbari, E., Azamathulla, H. & Mojallal, M. 2015 Estimation of scour depth below free overfall spillways using multivariate adaptive regression splines and artificial neural networks. *Engineering Applications of Computational Fluid Mechanics* **9**, 291–300.

Saneie, M., Sheikh Kazemi, J. & Azhdary Moghaddam, M. 2016 Scale effects on the discharge coefficient of ogee spillway with an arc in plan and converging training walls. *Civil Engineering Infrastructures Journal* **49**, 361–374.

Savage, B. M. & Johnson, M. C. 2001 Flow over ogee spillway. Physical and numerical model case study. *J. Hydraul. Eng. ASCE* **127**, 641–649.

Shahheydari, H., Nodoshan, E. J., Barati, R. & Moghadam, M. A. 2015 Discharge coefficient and energy dissipation over stepped spillway under skimming flow regime. *KSCE Journal of Civil Engineering* **19**, 1174–1182.

Shiri, J., Kisi, O., Yoon, H., Lee, K.-K. & Nazemi, A. H. 2013 Predicting groundwater level fluctuations with meteorological effect implications – a comparative study among soft computing techniques. *Computers & Geosciences* **56**, 32–44.

Shiri, J., Marti, P. & Singh, V. P. 2014 Evaluation of gene expression programming approaches for estimating daily evaporation through spatial and temporal data scanning. *Hydrological Processes* **28**, 1215–1225.

Skogerboe, G. V., Hyatt, M. L., Anderson, R. K. & Eggleston, K. O. 1967 *Design and Calibration of Submerged Open Channel Flow Measurement Structures: Part 3 – Cutthroat Flumes*. Report. Paper 86, Utah Water Research Laboratory, Utah, USA.

Tullis, B. P. 2010 Behavior of submerged ogee crest weir discharge coefficients. *Journal of Irrigation and Drainage Engineering* **137**, 677–681.

Tullis, B. & Neilson, J. 2008 Performance of submerged ogee-crest weir head-discharge relationships. *Journal of Hydraulic Engineering* **134**, 486–491.

US Army Corp of Engineers, USACE 1990 Hydraulic design of spillways. EM 1110-2-1603, Dept. of the Army, Washington, DC, USA.

Varshney, R. & Mohanty, S. 1973 Discharge relations for submerged weirs. *Indian Journal of Power* **23**, 225–228.

Zahiri, A. & Dehghani, A. 2009 Flow discharge determination in straight compound channels using ANN. *World Academy of Science, Engineering and Technology* **58**, 12–15.

Zahiri, A., Azamathulla, H. M. & Ghorbani, K. H. 2014 Prediction of local scour depth downstream of bed sills using soft computing models. *Computational Intelligence Techniques in Earth and Environmental Sciences* **197**. DOI 10.1007/978-94-017-8642-3_11.

First received 1 November 2018; accepted in revised form 17 January 2019. Available online 13 February 2019